AD-A186 006 EXPERIMENTAL AND THEORETICAL DETERMINATION OF J(1C) FOR 2024-T351 ALUMINUM ALLOY(U) AERONAUTICAL RESEARCH LABS MELBOURNE (AUSTRALIA) P W BEAVER ET AL. 1986 1/1

UNCLASSIFIED ARL-STRUC-R-420 F/G 11/6.1 NL

END

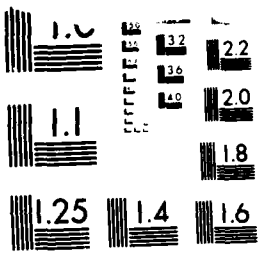

MICROCOPY RESOLUTION TEST CHART

(12)

ARL-STRUC-R-420 AR-004-481

AD-A186 006

DTIC FILE COPY

DEPARTMENT OF DEFENCE

DEFENCE SCIENCE AND TECHNOLOGY ORGANISATION

AERONAUTICAL RESEARCH LABORATORIES

MELBOURNE, VICTORIA

STRUCTURES REPORT 420

EXPERIMENTAL AND THEORETICAL DETERMINATION OF J_{IC} FOR 2024-T351 ALUMINIUM ALLOY

by

P.W.BEAVER, M.HELLER, and T.V.ROSE

DTIC
ELECTE
OCT 15 1987
S D
D

Approved for Public Release

DISTRIBUTION STATEMENT A
Approved for public release;
Distribution Unlimited

(C) COMMONWEALTH OF AUSTRALIA 1986

July 1986

87 10 6 057

AR-004-481

DEPARTMENT OF DEFENCE
DEFENCE SCIENCE AND TECHNOLOGY ORGANISATION
AERONAUTICAL RESEARCH LABORATORIES

STRUCTURES REPORT 420

EXPERIMENTAL AND THEORETICAL DETERMINATION OF J_{IC} FOR 2024-T351 ALUMINIUM ALLOY

by

P. W. BEAVER, M. HELLER, and T. V. ROSE

SUMMARY

The J-integral is an elastic-plastic fracture mechanics parameter which can be regarded as a measure of the intensity of the crack tip stress and strain fields, irrespective of the plastic zone size. The value of J at the onset of stable crack extension, J_{IC}, has been suggested as a fracture criterion for both large- and small-scale yielding conditions. In this work the value of J_{IC} for an extruded, medium-strength aluminium alloy, 2024-T351 bar, was determined using; (i) *the Hutchinson-Rice-Rosengren crack tip model and experimentally-determined crack tip strain profiles;* (ii) *a finite element-hybrid contour method,* (iii) *a modified linear elastic fracture mechanics approach, and* (iv) *the ASTM standard multiple- and single-specimen techniques. Agreement between the values obtained from the crack tip strain profile method, the two numerical methods and the multiple-specimen methods is good.*

The J_{IC} value determined by the single-specimen method is not valid as the amount of crack extension at each load level could not be determined to the accuracy required by the ASTM standard, using the recommended unloading compliance method.

© COMMONWEALTH OF AUSTRALIA 1986

POSTAL ADDRESS: Director, Aeronautical Research Laboratories,
Box 4331, P.O., Melbourne, Victoria, 3001, Australia

CONTENTS

	Page No.
1. INTRODUCTION	1
2. BACKGROUND	1
3. EXPERIMENTAL PROCEDURE	2
3.1 ASTM Standard Multiple- and Single-Specimen Test Methods	2
3.2 Crack Tip Strain Profile Method	5
4. NUMERICAL ANALYSIS	7
4.1 Finite Element-Hybrid Contour Method	7
4.2 Modified Linear Elastic Fracture Mechanics Method	7
5. RESULTS AND DISCUSSION	9
5.1 ASTM Standard Test Methods	9
5.2 Crack Tip Profile Method	11
5.3 Numerical Methods	15
6. CONCLUSIONS	17
ACKNOWLEDGMENTS	
REFERENCE	
DISTRIBUTION LIST	
DOCUMENT CONTROL DATA	

DTIC COPY INSPECTED 7

Accesion For
NTIS CRA&I ☑
DTIC TAB ☐
Unannounced ☐
Justification
By
Distribution /
Availability Codes
Dist | Avail and / or Special
A-1

1. INTRODUCTION

The application of linear elastic fracture mechanics (LEFM) to many practical situations is inappropriate because crack initiation and growth are usually accompanied by crack tip plasticity. As a result, considerable effort has been devoted to developing methods to characterize the fracture properties of metals in the elastic-plastic regime.

The J-integral, as initially proposed by Rice [1], is one elastic-plastic fracture mechanics parameter which has aroused considerable interest in recent years. It can be regarded as a measure of the intensity of the crack tip plastic stress and strain fields, similar to the stress intensity factor, K, in LEFM. Begley and Landes [2] first proposed that the onset of crack extension under plane strain conditions would occur when the J-integral exceeds a critical value J_{IC}. Since then considerable data have been published supporting the use of J_{IC} as an elastic-plastic fracture criterion.

This paper describes a test program to determine the J_{IC} value for an extruded medium-strength aluminium alloy, 2024-T351, which is used in the aircraft industry. This value was determined using: (i) the Hutchinson-Rice-Rosengren crack tip model and experimentally-determined crack tip strain profiles, (ii) a finite element-hybrid contour method, (iii) a modified linear elastic method, and (iv) the multiple- and single-specimen methods, as described in the ASTM standard E-813-81.

2. BACKGROUND

The justification for using J-integral as a ductile fracture criterion is based on the Hutchinson-Rice-Rosengren crack tip model, known as the HRR singularity [3, 4]. These authors determined the stress and strain distributions at the crack tip for non-linear elastic materials which display a Ramberg-Osgood relationship between the effective stress σ and effective plastic strain ε^p. The Ramberg-Osgood relationship is given by the following equation:

$$\sigma = \sigma_1[\varepsilon^p]^n \tag{1}$$

where n is the work hardening exponent and σ_1 is a constant. McClintock [5] showed, by combining the HRR model with Rice's definition of J, that the crack tip plastic stress and strain fields can be expressed as a function of J as follows:

$$\sigma^p_{ij} = \sigma_1(J/\sigma_1 \cdot I_n)^{n/(n+1)} \cdot r^{-n/(n+1)} \cdot \tilde{\sigma}_{ij}(\theta) \tag{2}$$

and

$$\varepsilon^p_{ij} = (J/\sigma_1 \cdot I_n)^{1/(n+1)} \cdot r^{-1/(n+1)} \cdot \tilde{\varepsilon}^p_{ij}(\theta) \tag{3}$$

where r and θ are the polar co-ordinates, I_n is a function of n and stress state, and $\tilde{\sigma}_{ij}(\theta)$ and $\tilde{\varepsilon}^p_{ij}(\theta)$ are universal functions of θ, and which also depend on n and stress state. The exact forms of Equations (2) and (3) depend on the stress-strain law used to represent the material behaviour, and whether or not non-dimensionalizing factors are used. Consequently, several variations of these equations have been published in the literature, for example see References 6–8. In this work, the forms of the equations as derived originally by McClintock are used.

Comparison of the plastic stress and strain equations with the elastic stress field equations from LEFM reveals that they are of the same form. Moreover, for the case when $n = 1$ (linear elastic behaviour) Equations (2) and (3) reduce to the linear elastic fracture mechanics $1/r^{1/2}$ singularity.

The underlying assumptions used in deriving the HRR equations, however place some limitations on the use of J as a fracture criterion. Firstly, the material behaviour is assumed to conform to the deformation theory of plasticity, that is, the material behaves as a non-linear elastic solid and no unloading occurs during deformation. When crack extension occurs in real materials, some unloading takes place in the wake of the new crack tip [9]. Hence, the first limitation is that J can only be used to represent crack initiation under monotonic loading. However, in recent years J has been used for predicting fatigue crack growth with success which suggests that this limitation may be relaxed, for example see References 10 and 11. A second consideration in using J is that the region ahead of the crack tip in which J describes the stress-strain field must be large compared with the microstructural elements of deformation and fracture. These processes occur in an intensely-deformed region at the crack tip, the size of which is of the order of the crack tip opening displacement (CTOD), as will be discussed later. Therefore, the radius of the region dominated by the HRR field must be large compared with the CTOD.

3. EXPERIMENTAL PROCEDURE

Aluminium alloy 2024-T4 extruded bars of rectangular cross-section (108 mm × 11 mm) were rolled to 6·4 mm thickness and heat treated to the T351 condition. The average tensile properties after this treatment were: 0·2% proof stress 426 MPa, ultimate stress 503 MPa and total elongation 17·2%. The specimen geometry used in this work was a modified compact tension specimen, as shown in Fig. 1. Numerically-determined compliance curves have shown that this specimen is more compliant at shorter crack lengths than an ASTM compact tension specimen of the same dimensions [12].

3.1 ASTM Standard Multiple- and Single-Specimen Test Methods

The J_{IC} value for 2024-T351 was determined using the multiple- and single-specimen test methods as specified in the ASTM standard E813-81. Briefly, these methods can be described as follows:

In the multiple-specimen method, several specimens, all with the same size of fatigue crack, are given different values of tensile load and then unloaded. The amount of stable crack extension, Δa, for each specimen is determined by first marking the crack front, and then completing the fracture statically so that the amount of crack extension can be observed. (Crack fronts in aluminium alloys are usually marked by fatigue cycling at low loads whereas heat tinting is used for steels. During this research program a more effective method of marking crack fronts in aluminium alloys was developed. This new method, based on liquid metal embrittlement of grain boundaries in aluminium by gallium, is described in Reference 13)..

The single-specimen technique differs from the multiple-specimen technique in that the Δa values are estimated from the unloading slope of the load displacement curve and the elastic compliance [14]. The unloading slope is determined at several values of load during the test. This method assumes that small amounts of unloading, i.e. of the order of 10% of the load, will not disturb the fracture process but will provide a small portion of a linear elastic curve whose slope will give an instantaneous measure of the crack length. The compliance calibration curve used in this work is given in Reference 12.

The values of J for each Δa value in both techniques are determined using the area under the load versus load-line displacement curve, A, (Fig. 2(a)) and the following equation:*

$$J = A \cdot f(a_0/W)/(B \cdot b) \tag{4}$$

where $f(a_0/W)$ is a dimensionless coefficient which is a function of the initial crack length a_0 and the specimen width W, B is the specimen thickness and b is the remaining ligament width.

* Please note that the formulation of Equation 4 in the ASTM standard is misleading, the coefficient $f(a_0/w)$ should be in the numerator.

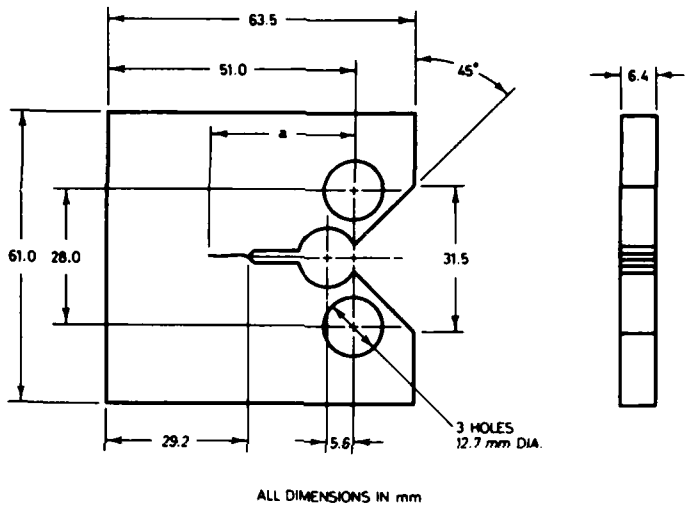

Fig. 1 J-integral specimen.

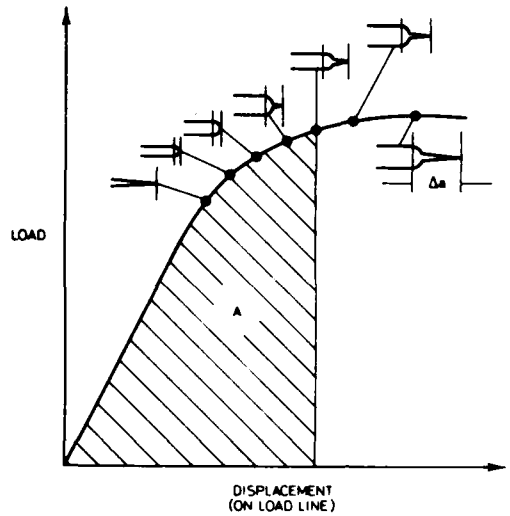

a) Several specimens are loaded to different values and the corresponding J values are determined from the areas under the load/displacement curve.

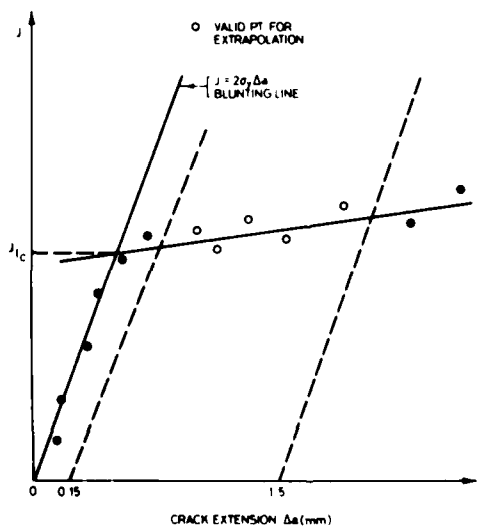

b) A J-resistance curve is constructed using the values of J determined in (a) and the corresponding crack extension (Δa) values determined from the fracture surfaces.

Fig. 2 Schematic diagram of the procedure for determining J_{1C} using the ASTM standard multiple specimen test method.

A J-resistance curve is then constructed by plotting the values of J for each load level as a function of Δa, as shown schematically in Fig. 2(b).

A crack tip blunting line, which represents an amount of crack extension from stretching of the crack tip, (as distinct from fracture) is also drawn on the J-resistance curve. This blunting line is approximated by the following equation

$$J = 2\sigma_y \cdot \Delta a \tag{5}$$

where σ_y is the yield strength. In addition, 0·15 mm and 1·5 mm offsets are drawn parallel to the blunting line. The ASTM standard requires that at least 4 data points fall within these two offset lines. The critical J_{IC} value can then be determined from the point of intersection of a linear regression line fitted to these data and the blunting line. This point represents the onset of stable crack extension from the blunt crack tip.

3.2 Crack Tip Strain Profile Method

J can also be determined from the crack tip strain distributions at various points on the load/displacement curves using a photo-printed square grid (40 lines/mm) on the specimen surface and a replicating technique, as outlined in Reference 15. Microgrid patterns were applied to the surfaces of the specimens used in the ASTM single-specimen tests. The variation in the spacing of grid lines was less than 0·1 μm. An example of a photo-printed grid, on a specimen which has been fatigue cracked, is shown in Fig. 3. The onset of stable crack extension could also be determined from the replicas, and hence the critical load for first stable crack extension P_c and the J_{IC} value can be determined, as will be described later.

The values of J at the points on the load/displacement curve at which replicas were taken were determined from the plastic strain profiles ahead of the crack tip, $\varepsilon^p_{yy}(\theta = 0)$ versus r data, using a 75 μm gauge length and Equation (3). An example of a typical plastic strain profile is shown in Fig. 4. However, strain values within the so-called intensely deformed zone [7] were not used as it is not clear whether Equation 3 is valid in this region. The extent of the intensely deformed zone in front of the crack tip is approximately

$$w = \text{M.CTOD} \tag{6}$$

where M is a constant with a value of 1[16] or 2[7], and the CTOD is given by the following equation

$$\text{CTOD} = N.J\,\sigma_y \tag{7}$$

where N is a constant. Broek [17] found that $N = 0{\cdot}44$ for aluminium alloys so that at the critical load CTOD $\cong$ 20 μm which is within the experimentally determined range of values using the replicas. In the present work no strain value within 40 μm of the crack tip was used in determining the J values. Furthermore, results from a theoretical analysis of Shih and German [18] showed that, for compact tension specimens, the HRR singularity is only valid over distances from the crack tip of 6–10 times the CTOD value. Therefore, no strain value greater than approximately 200 μm was used to determine the J values.

The values of J at each load level were determined using the strain values within the above range of r values and Equation (3). The values of σ_1 and n in Equation (3) were determined using tensile test data for the same material and Equation (1); these values are 678 MPa and 0·075 respectively. Values of I_n and $\tilde{\varepsilon}^p_{ij}(\theta)$ are given in Reference 5; for a tensile crack under plane stress conditions, and an n value of 0·077 (the nearest tabulated value of n to 0·075), $I_n = 2{\cdot}87$ and $\tilde{\varepsilon}^p_{ij}(\theta = 0) = 0{\cdot}8$. (It should be noted that, even though the specimen geometry satisfied the ASTM requirements for plane strain conditions, plane stress values of I_n and $\tilde{\varepsilon}^p_{yy}(\theta = 0)$ were appropriate as the strain profiles are from surface measurements).

The values of J for the same load displacement points at which the replicas were taken were also determined using the area under the curve as for the multiple-specimen technique. These values were then compared with the values determined from the crack tip strain profiles.

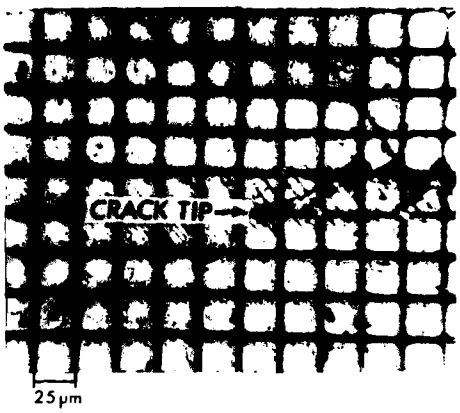

Fig. 3 An example of a photo-printed grid used to measure the strains ahead of crack tips. This photograph is of the fatigue precracked J-integral specimen number BP27 prior to loading. The lines at 45° to the crack are intensive slip bands produced during the precracking.

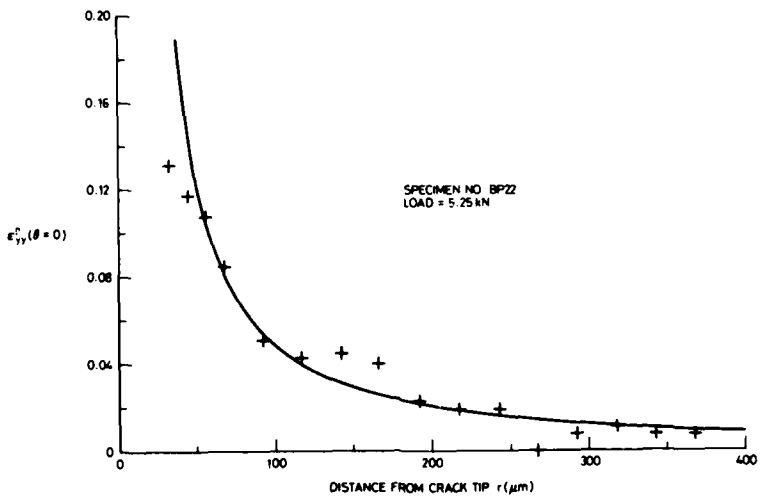

Fig. 4 A typical crack tip plastic strain profile as determined from replicas of a photo-printed square grid on the specimen surface.

4. NUMERICAL ANALYSIS

Two numerical methods, both assuming plane strain, were used to evaluate J for the specimen geometry used in the experimental work. Values of crack length, a and the load at initial stable crack extension P_s were obtained from the experimental results for the single-specimen tests; for specimen number BP22 $a = 25 \cdot 55$ mm and $P_s = 5 \cdot 25$ kN and for specimen number BP27 $a = 25 \cdot 10$ mm and $P_s = 5 \cdot 98$ kN. Both numerical approaches used the finite element method, with the analyses being done using the PAFEC suite of programs. The stiffness matrices were computed using 2×2 reduced integration and double precision, and the solution was obtained using double precision.

4.1 Finite Element—Hybrid Contour Method

In this method the value of J was determined using the displacement results of an elastic-plastic finite element analysis and applying the hybrid contour method [19]. The finite element mesh used, shown in Fig. 5(a), consisted of 212 eight-noded iso-parametric quadrilateral elements and 11 six-noded isoparametric triangular elements. To represent the loading applied during testing, a point load, P, was applied at the top of the pin hole. (It has been demonstrated in Reference 12 that the stresses in the crack tip region are insensitive to whether a point or distributed loading is applied at the hole). The stress-strain properties of the material were approximated by assuming a two-segment piece-wise linear relation. For accurate modelling of the plasticity effects surrounding the crack tip, special crack tip elements were used, and the total load was applied in increments. The relevant details are as follows:

(i) In the region surrounding the crack tip the mesh is particularly refined, with the two crack tip elements being approximately 1/60th the length of the crack, a. These two elements had their midside nodes shifted to the quarter points to generate the near-tip $r^{1/2}$ displacement singularity [20]. Various studies have shown that these elements give very good results when used for both elastic and plastic crack tip conditions [21, 22].

(ii) The first load increment was chosen to, approximately, coincide with the load that first caused a near tip gauss point to become plastic. The remaining increments each corresponded to 5% of the total load. A solution convergence to less than 1·3% error in stresses was achieved.

In the hybrid contour method the nodal displacements along a contour in the elastic material surrounding the crack tip plastic zone were used to evaluate J (These nodal displacements were determined in the finite element analysis). The contour used in shown in Fig. 5(b) along with the plastic zone as also determined from the finite element analysis.

4.2 Modified Linear Elastic Fracture Mechanics Method

In this approach it was assumed that the presence of crack tip plasticity makes the specimen behave as if it contained an elastic crack larger than the actual size of the crack, a. Hence the effective crack size, a_{eff}, is taken to equal $a + r_p/2$, where r_p is an estimate of the plastic zone length [23], and is given by

$$r_p = \frac{K^2}{\pi (1 \cdot 68\, \sigma_y)^2} \tag{8}$$

where K is the mode I stress intensity factor.

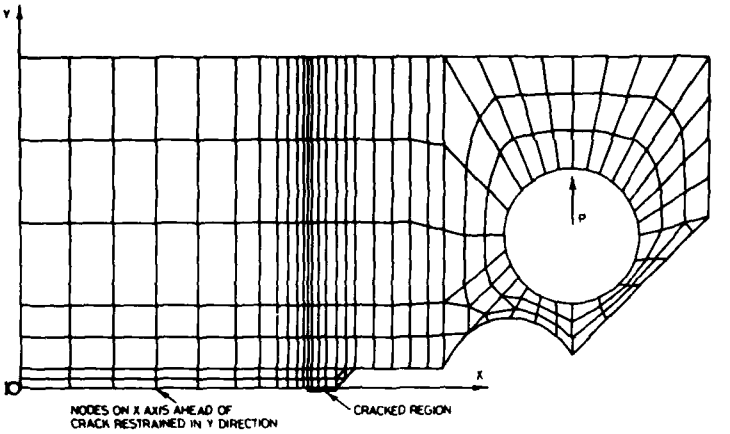

(a) Finite element mesh (half of specimen modelled).

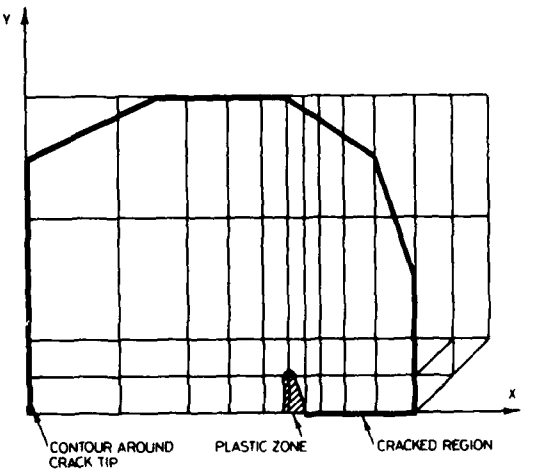

(b) Contour used to compute J.

Fig. 5 Finite element modelling.

An iterative procedure was used to estimate the value of K at the crack length a_{eff} for both specimens BP22 and BP27. Initially, r_p was determined using K based on the actual crack length, a revised K was then estimated for a crack length of $a_{eff} = a + r_p/2$. The various values of K were determined from the displacements (obtained from elastic finite element analyses) of nodal points behind the crack tip using the equation given in Reference 24, namely,

$$K = \frac{uE}{4(1 - \nu^2)} \cdot \sqrt{\frac{2\pi}{r}} \tag{9}$$

where u is the load direction displacement of a near tip node on the crack face behind the crack tip, r is the distance of that node from the crack tip and E is Young's modulus.

Finally, the value of J was evaluated using the estimated value of K by substituting into the equation relating J and K for elastic plane strain conditions,* namely,

$$J = \frac{K^2}{E}(1 - \nu^2) \tag{10}$$

where ν is Poisson's ratio. The values of E and ν for 2024-T351 are $E = 72{\cdot}4$ GPa and $\nu = 0{\cdot}31$.

5. RESULTS AND DISCUSSION

5.1 ASTM Standard Test Methods

A J_{IC} value of $16{\cdot}9$ kJ/m^2 was first determined using the J-resistance curve constructed from the multiple-specimen test data as shown in Fig. 6. This value is in good agreement with the estimated J_{IC} value of $18{\cdot}0$ kJ/m^2 obtained using equation 10 and the K_{IC} value of $38{\cdot}5$ MPa$\sqrt{m}$ for this alloy as given in Reference 25.

The J_{IC} value determined from the single-specimen J-resistance curve, shown in Fig. 6, is $47{\cdot}8$ kJ/m^2. This value is much higher than the values obtained from both the multiple-specimen test data and the estimated J_{IC} value. The large difference between the single- and multiple-specimen J_{IC} values is unexpected and suggests that the Δa values were not accurately determined using the unloading compliance. This was verified using data from the multiple-specimen tests. The Δa values for specimens used in these tests were estimated using the final unloading compliances and were compared with the values measured from the fracture surfaces. The Δa values determined from the complaince values were at least 27% less than those measured directly from the fracture surface. Therefore, the single-specimen J_{IC} value is not valid as the ASTM standard requires that the difference between the estimated and real Δa values must be less than 15%.

Three factors were identified as being responsible for the large difference between the estimated and real Δa values, these are:

1. *non-linearities in the mechanical and electrical systems,*

2. the sensitivity of the compliance calibration, and

3. crack tunnelling effects.

---

* It should be noted that the computer program used to determine the values of K could simulate elastic plane strain conditions even though the specimens were only 6·4 mm thick. (This specimen thickness satisfies the ASTM requirements for a valid plane strain J_{IC} test whereas it does not satisfy the ASTM requirements for valid linear elastic plane strain K_{IC} test.)

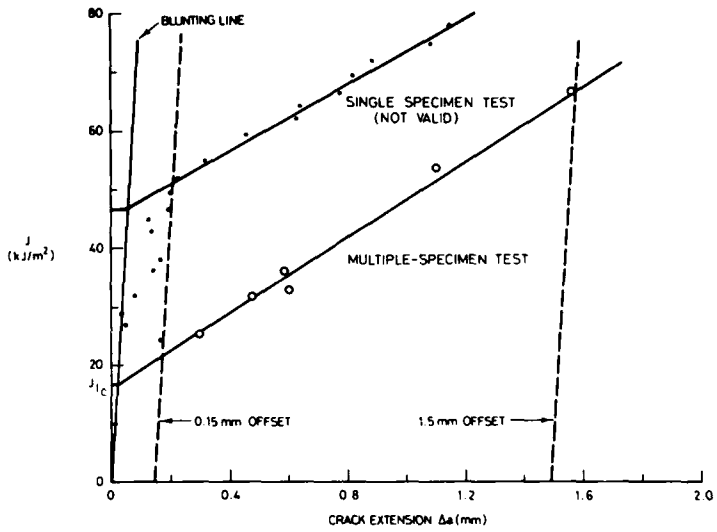

Fig. 6 J-resistance curve for 2024-T351 as determined by the ASTM multiple and single specimen test methods.

The first factor is a result of the method used to measure the unloading compliance. The recommended method is to electronically subtract the elastic part of the load-displacement curve and replot the non-linear part with a higher amplification. This amplification improves the accuracy of the measurements; however small non-linearities in the mechanical or electrical system become apparent during the unloadings. For example, clip gauge hysteresis, and friction between the clip gauge and knife edges, the specimen and loading pins, and the loading pins and clevises result in non-linearities and make it difficult to estimate the best fit lines for the unloading curves. The errors in measuring the unloading compliance are of the order of 2%, however, the resulting errors in the estimated Δa values are up to 100%, i.e. the compliance calibration is very sensitive to small changes in the unloading compliance value. The sensitivity of the compliance calibration can be reduced by using longer initial crack lengths, that is if the a/W ratio is increased from 0·5 to 0·7, where W is the specimen width.

Examination of the fracture surfaces after the various tests showed crack tunnelling which affects the unloading compliance and hence the Δa values. When the crack front is curved, the crack does not close uniformly during unloading as it is not closing along a straight hinge line. This uneven closure means that the unloading compliance value is higher as the shift in the rotation point is retarded compared with the situation when the crack front is straight and closure uniform. Therefore, the estimated Δa values are less than the real values as determined by direct measurement [26] and this results in the J-integral values being over-estimated. Crack tunnelling is very difficult to prevent although it can be minimised by using side-grooved specimens or thicker specimens.

5.2 Crack Tip Strain Profile Method

Crack tip strain distributions were determined from replicas of the surface grid patterns, examples of which are shown in Figs 7(a)–(d) for specimen BP27. The plastic strain profiles ahead of the crack tip (ε_{yy}^{p} vs r) determined from these replicas are shown in Fig. 8. This figure shows that the shape of the plastic strain profile changes when significant crack extension occurs.

The values of J at each load level were determined by substituting the strain values at distances of between approximately 40 and 200 μm from the crack tip into Equation (3). These data showed that the several values of J at each load level were essentially the same. The mean values of J at each load level, denoted J_{STRAIN}, and the standard deviations for the two specimens used for this technique are given in Table 1. These results support the analytical results of Shih and German [18] that the HHR singularity is valid for distances from the crack tip of up to 10 times the COD value for compact tension specimens.

The values of J at each load level were also determined from the areas under the load–displacement curves, denoted as J_{AREA}, and are given in Table 1. Agreement between the J_{STRAIN} and J_{AREA} values at each load level is good except at the lower load levels for specimens BP22.

The load at which stable crack extension first occurred and the associated J_{IC} value were established by examining the replicas of the crack tips and the associated grid patterns in both an optical and a scanning electron microscope. As mentioned in the Introduction, as soon as initial crack extension occurs, the material behind the new crack tip starts to unload. This phenomenon can be seen in Figs 7(a)–(d). As the load is increased from 5·07 to 5·77 kN the CTOD and the width of the secondary crack, region A, also increased, Figs 7(a) and (b). However, as the load is further increased to 6·20 kN the CTOD and the width of region A decreased significantly, Figs 7(b) and (c). This change in the crack profile is a result of the unloading associated with initial crack extension in the interior of the specimen. (It should be noted that this unloading behind the crack tip did not relax the surface strains ahead of the crack tip, as shown by the strain profiles, in Fig. 8 corresponding to the above micrographs.) A small amount of crack extension also occurred at the surface. Crack extension occurs first in the interior of the specimen as the triaxial stress state increases the maximum principal stress up to three times the uniaxial yield stress. In comparison, the maximum principal stress at the surface is limited to approximately the yield stress. On further increasing the load from 6·20 to 6·50 kN, Figs 7(c) and (d), significant crack extension occurs at the surface, and the CTOD increases although the width of the secondary crack decreases.

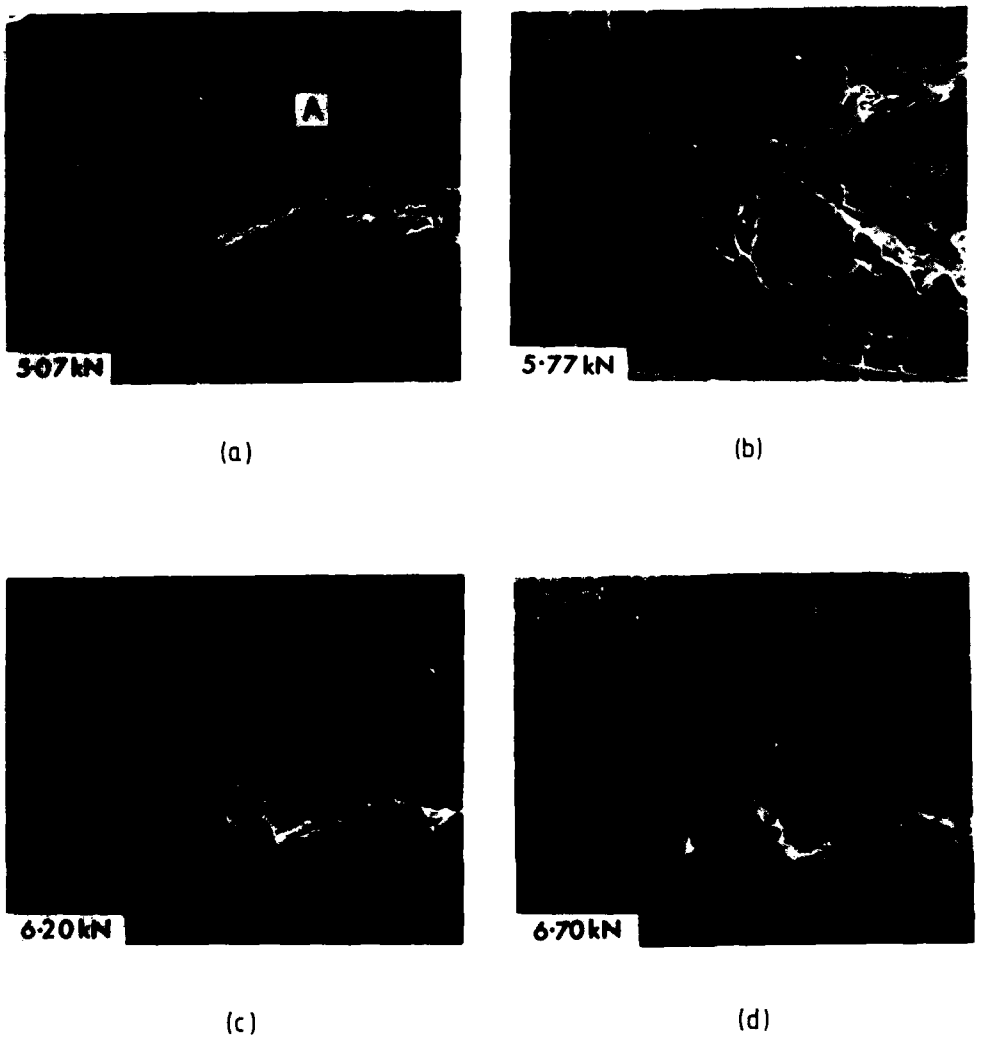

Fig. 7 Replicas of the crack tip profiles and grid distortions for specimen BP27 at various loads. (a) 5.07 kN, (b) 5.77 kN, (c) 6.20 kN, and (d) 6.70 kN (elastic limit = 4.80 kN).

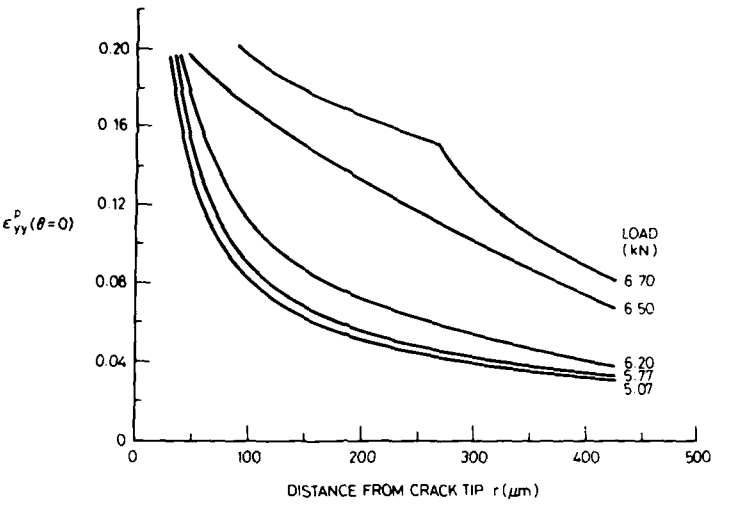

Fig. 8 Crack tip plastic strain profiles for specimen BP27.

TABLE 1

J-Integral Values at Several Points on the Load Versus Load-Line Displacement Curves as Determined from (a) Crack Tip Profiles, and (b) The Area Under the Curve

Specimen Number and Crack Length	Load (kN)	J_{STRAIN} (kJ/m^2)		J_{AREA} (kJ/m^2)	
		Mean	Standard Deviation	Mean	Standard Deviation
BP22	4·45	10·5	2·2	14·4	0·6
a_i = 25·55 mm	4·88	12·8	2·5	17·8	0·7
	5·25	20·0	2·7	21·4	0·9
	5·63	≅ 70 μm surface crack growth		25·5	1·0
BP27	5·07	19·7	2·5	18·0	0·7
a_i = 25·10 mm	5·77	21·2	2·3	22·1	0·9
	6·20	22·4	1·5	25·0	1·0
	6·70	≅ 40 μm surface crack growth		34·3	1·4

The above micrographs show that initial crack extension occurred in specimen BP27 at a load between 5·77 kN and 6·20 kN, hence J_{IC} is between 21·2 and 22·4 kJ/m^2. An estimate of the J_{IC} value can be obtained by assuming that initial crack extension occurred at a load midway between the above values. This produces a J_{IC} value for specimen BP27 of about 21·8 kJ/m^2. Similarly, the replicas showed that initial crack extension in specimen BP22 occurred at a load between 5·25 kN and 5·63 kN. However, the J value at the higher load level could not be determined as the amount of crack growth at this load level significantly altered the crack tip strain profile. Therefore, a lower bound estimate of the J_{IC} value for specimen BP22 is 20·0 kJ/m^2.

The accuracy of this technique obviously depends on the load intervals at which the replicas are taken. The best procedures to estimate J_{IC} are to either, estimate the critical load using the lower bound LEFM estimate of J_{IC}, and take two to three replicas at load increments approximately 5% on either side of P_s, or to use an additional specimen to experimentally determine P_s. More replicas would be required for this specimen than for subsequent specimens.

As mentioned in Section 3, the J_{IC} values determined from the surface crack tip strain profiles are for plane stress conditions, whereas the value obtained from the ASTM multiple-test method is for plane strain. Under elastic conditions, the plane strain J_{IC} value is less than the plane stress value by a factor of $(1 - \nu^2)$ [16]. The value of ν for this alloy is 0·31 so that

$$J_{IC}\,(\text{plain strain}) = 0{\cdot}90.J_{IC}\,(\text{plane stress}) \tag{11}$$

This equation can be used to give an estimate of the plane strain J_{IC} values using the plane stress values obtained from the crack tip strain profile method as initial crack extension was associated with only a small amount of plastic deformation. These plane strain J_{IC} values are in good agreement with the J_{IC} value obtained from the multiple-specimen test. As shown in Table 2(a) the 95% confidence intervals for the two methods overlap indicating that the differences between the J_{IC} values are due to material variability and experimental scatter.

5.3 Numerical Methods

J_{IC} values were also determined using the two numerical methods outlined in Section 4. As shown in Table 2(b), the J_{IC} values determined from the hybrid-contour and the modified LEFM methods are nearly identical for each specimen. The differences between the values for the two specimens are a result of the errors associated with determining the load P_c and material variability.

TABLE 2
J_{IC} Values Determined By Various Methods

Method	Specimen Number	Stress State	J_{IC} (kJ/m^2)	95% Confidence Interval (kJ/m^2)
(a) *Experimental*				
Single specimen test	—	plane strain	47·8 (not valid)	
Multiple specimen test	—	plane strain	16·9	12·1–21·7
Crack tip strain Profile method	BP22	plane stress	≧20·0	13·8–26·2
	BP27	plane stress	21·8	16·2–27·4
	BP22	plane strain*	≧18·0	12·4–23·6
	BP27	plane strain	19·6	14·6–24·7
(b) *Numerical*				
FEM hybrid-contour method	BP22	plane strain	17·8	14·5–26·1
	BP27	plane strain	22·5	
Modified LEFM approach	BP22	plane strain	18·1	
	BP27	plane strain	22·5	
Using K_{IC} from Ref. 25 & eqn 10	—	plane strain	18·0	

* Estimates of the plane strain J_{IC} values were obtained from the plane stress values using equation 11.

The determination of J_{IC} using the modified LEFM approach is based on the assumption that Equation 10, which comes from the linear elastic definition of J, is valid in the elastic-plastic regime; that is, if the amount of plastic deformation is small enough J_{IC} will be identical to G_{IC} and hence can be related to K_{IC}. However, J_{IC} is experimentally determined using small specimens which reach the fracture point well beyond the linear elastic regime. In comparison, K_{IC} is experimentally determined using thicker specimens which reach the fracture point under linear elastic conditions. This means that the measurement point for J_{IC}, i.e. at initial stable crack extension, may not be coincident with the measurement point for K_{IC}, i.e. at 2% crack extension, especially if there is significant plastic deformation [27]. Landes and Begley [27] used the R-curve to illustrate this difference in measurement point between the two methods. For a standard ASTM linear elastic K_{IC} test the R-curve is nearly flat so that the K_{IC} value at 2% extension is approximately the same as the value of K at initial crack growth, as shown schematically in Fig. 9. Consequently, Equation 10 is valid as the measurement points for both K_{IC} and J_{IC} are comparable. In comparison for materials which fail by a ductile mechanism or for thin sheet "plane stress" behaviour, the R-curve can be fairly steep. The K_{IC} value at 2% extension for these situations would not be the same as the K taken at initial crack extension Fig. 9. This means that the J_{IC} measured at the point of initial crack growth would be lower than the J_{IC}

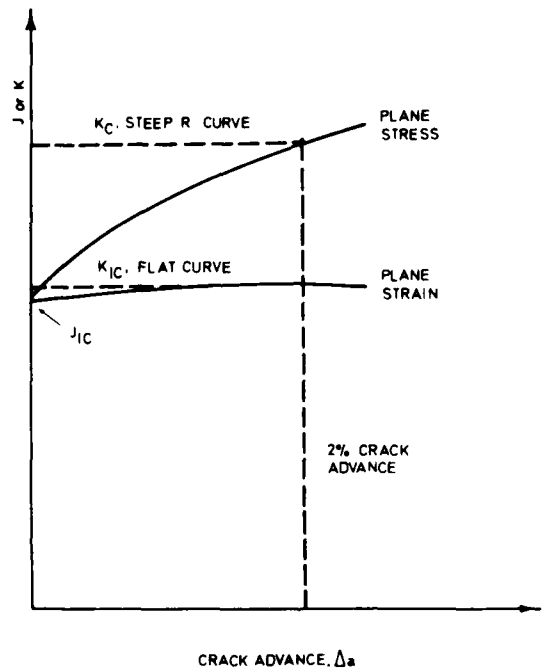

Fig. 9 Schematic of R-curve showing the differences between the J_{1C} and K_{1C} measurement points [27].

value determined from K_{IC} at 2% crack extension. However, in this work the load at which first stable crack growth occurred P_s, as determined from the replicas, was used to calculate K, denoted as K_s, and not the load at 2% extension or P_{CRIT}. Therefore, the values of J determined from the K_s values using the modified LEFM approach will be consistent with the J_{IC} values determined using the crack tip strain profile method. Table 2 shows that the J_{IC} values obtained by the two methods are in agreement.

6. CONCLUSIONS

The J_{IC} value for extruded, medium strength 2024-T351 aluminium alloy has been determined using three experimental and two theoretical methods. Agreement between the J_{IC} values obtained from (i) a crack tip strain profile method, (ii) a finite element-hybrid contour method, (iii) a modified linear elastic farcture mechanics approach and (iv) the ASTM multiple-specimen technique is good.

The J_{IC} value determined by the single-specimen technique is not valid as the amount of crack extension at each load level could not be determined to the accuracy required by the ASTM standard, using the recommended unloading compliance method.

ACKNOWLEDGMENTS

The authors would like to thank Dr G. Clark and Dr R. Jones for their helpful discussions and interest shown in this work, Mr R. Pell for his assistance with the scanning electron microscopy and Drs J. M. Finney and C. K. Rider for their constructive comments on the manuscript of this paper.

REFERENCES

1. Rice, J. R., A path independent integral and the approximate analysis of strain concentrations by notches and cracks, *J. Appl. Mech.*, *35*, 1968, 379–386.

2. Begley, J. A. and Landes, J. D., The effect of specimen geometry on J_{IC}, in *Fracture Toughness, ASTM STP 514*, American Society for Testing and Materials, Philadelphia, 1972, 24–39.

3. Hutchinson, J. W., Singular behaviour at the end of a tensile crack in a hardening material, *J. Mech. Phys. Solids*, *16*, 1968, 13–31.

4. Rice, J. R. and Rosengren, G. F., Plane strain deformation near a crack tip in a power law hardening material, *J. Mech. Phys. Solids*, *16*, 1968, 1–12.

5. McClintock, F., Plasticity effects of fracture, in *Fracture – An Advanced Treatise Vol. 3*, Ed. H. Liebowitz, Academic Press, New York, 1971, 47–225.

6. Turner, C. E., Yielding fracture mechanics, *J. Strain Analysis*, *10*, 1975, 207–216.

7. Paris, P. C., Fracture mechanics in the elastic-plastic regime, in *Flaw Growth and Fracture, ASTM STP 631*, American Society for Testing and Materials, Philadelphia, 1977, 3–27.

8. Broek, D., *Elementary Engineering Fracture Mechanics*, Martinus Nijhoff Publishers, The Hague, 1984, 235–237.

9. Broek, D., *Elementary Engineering Fracture Mechanics*, Martinus Nijhoff Publishers, The Hague, 1984, 239.

10. Dowling, N. E. and Begley, J. A., Fatigue crack growth during gross plasticity and the *J*-integral, in *Mechanics of Crack Growth, ASTM STP 590*, American Society for Testing and Materials, Philadelphia, 1976, 82–103.

11. Dowling, N. E., Geometry effects and the *J*-integral approach to elastic-plastic fatigue crack growth, in *Cracks and Fracture, ASTM STP 601*, American Society for Testing and Materials, Philadelphia, 1976, 19–32.

12. Heller, M. and Paul, J., Numerical compliance and stress intensity factor calibrations of MRL compact specimens, *ARL Structures Tech. Memo 421*, 1985.

13. Beaver, P. W., *J*-integral testing of aluminium alloys—a new method for accurately marking crack fronts, *ARL Structures Tech. Memo.* 439, 1986.

14. Clarke, G. A., Andrews, W. R., Paris, P. C. and Schmidt, D. W., Single specimen tests for J_{IC} determination, in *Mechanics of Crack Growth, ASTM STP 590*, American Society for Testing and Materials, Philadelphia, 1976, 27–42.

15. Beaver, P. W., An evaluation of microgridding techniques for measuring local plastic strain distributions, *ARL Structures Tech. Memo.*, (in publication).

16. Ritchie, R. O., Why ductile fracture mechanics?, *J. Engng. Mater. Technol. (Trans of the ASME)*, *105*, 1983, 1–7.

17. Broek, D., Correlation between stretch zone size and fracture toughness, *Engng. Fract. Mech.* *6*, 1974, 173–181.

18. Shih, C. F. and German, M. D., Requirements for a one parameter characterization of crack tip fields by the HRR singularity, *Int. J. Fract.*, *17*, 1981, 27–43.

19. Jones, R., Watters, K. C. and Callinan, R. J., A hybrid contour method, *J. Struct. Mech.*, *13(1)*, 1985, 67–76.

20. Henshel, R. D. and Shaw, K. G., Crack tip elements are unnecessary, *Int. J. Num. Methods Engng*, *9*, 1975, 495–507.

21. Fawkes, A. J., Owen, D. R. J. and Luxmore, A. R., An assessment of crack tip singularity models for use with isoparametric elements, *Engng. Fract. Mech.*, *11*, 1979, 143–159.

22. Barsoum, R. S., Triangular quarter-point elements as elastic perfectly plastic crack tip elements, *Int. J. Num. Methods Engng*, *11*, 1977, 85–98.

23. Broek, D., *Elementary Engineering Fracture Mechanics*, Martinus Nijhoff Publishers, The Hague, 1984, 107.

24. Sih, G. C. and Liebowitz, H., Mathematical theories of brittle fracture, in *Fracture, An Advanced Treatise, Vol. 2*, Mathematical Foundations, Ed. H. Liebowitz, Academic Press, 1971, 92–93.

25. *Damage Tolerant Design Handbook, MCIC-HB-01R Vol. 3*, Metals and Ceramics Information Centre, Battelle Columbus Laboratories Ohio, 1983, 7-5-25.

26. Joyce, J. A. and Gudas, J. P., Computer interactive J_{IC} testing of Navy alloys, in *Elastic-Plastic Fracture Mechanics, ASTM STP 668*, American Society for Testing and Materials, Philadelphia, 1979, 451–468.

27. Landes, J. D. and Begley, J. A., Recent developments in J_{IC} testing, in *Developments in Fracture Mechanics Test Methods Standardization, ASTM STP 632*, American Society for Testing and Materials, Philadelphia, 1977, 57–81.

DISTRIBUTION

AUSTRALIA

DEPARTMENT OF DEFENCE

Defence Central

Chief Defence Scientist
Deputy Chief Defence Scientist (shared copy)
Superintendent, Science and Program Administration (shared copy)
Controller, External Relations, Projects & Analytical Studies (shared copy)
Counsellor (Defence Science) (London) (Doc. Data sheet only)
Counsellor Defence Science (Washington) (Doc. Data sheet only)
Defence Science Representative (Bangkok)
Defence Central Library
Document Exchange Centre, DISB (18 copies)
Joint Intelligence Organisation
Librarian H Block, Victoria Barracks, Melbourne
Director General—Army Development (NSO) (4 copies)

Aeronautical Research Laboratories

Director
Library
Divisional File—Structures
Authors: P. W. Beaver
M. Heller
A. A. Baker
G. Clark
F. G. Harris
J. M. Finney
B. C. Hoskin
R. Jones
G. S. Jost
A. S. Machin
J. Y. Mann
L. R. F. Rose
B. J. Wicks
D. G. Ford
C. K. Rider

Materials Research Laboratories

Director/Library
Dr S. Bandopadhyay

Defence Research Centre

Library

Navy Office

Navy Scientific Adviser
RAN Aircraft Maintenance and Flight Trials Unit
Directorate of Naval Aircraft Engineering
Director Naval Air Warfare
Superintendent, Aircraft Maintenance and Repair
Directorate of Naval Ship Design

Army Office

Scientific Adviser—Army
Engineering Development Establishment
  Library
  Mr S. Austin
Royal Military College Library
US Army Research, Development and Standardisation Group

Air Force Office

Air Force Scientific Adviser
Aircraft Research and Development Unit
  Scientific Flight Group
  Library
Technical Division Library
Director General Aircraft Engineering—Air Force
Director General Operational Requirements—Air Force
HQ Operational Command (SMAINTSO)
HQ Support Command (SLENGO)
RAAF College, Point Cook

Central Studies Establishment

Information Centre

Government Aircraft Factories

Manager
Library

Department of Aviation

Library
Flight Standards Division
Mr C. Torkington

Statutory and State Authorities and Industry

Trans-Australia Airlines, Library
Gas & Fuel Corporation of Vic., Manager Scientific Services
SEC of Vic., Herman Research Laboratory
  Library
  Dr R. Coade
BHP, Melbourne Research Laboratories
Hawker de Havilland Aust. Pty Ltd, Victoria, Library
Hawker de Havilland Aust. Pty Ltd, Bankstown, Library

Universities and Colleges

Adelaide
  Barr Smith Library
  Professor of Mechanical Engineering

Flinders
Library

La Trobe
Library

Melbourne
Engineering Library

Monash
Hargrave Library
Professor I. J. Polmear, Materials Engineering

Australian Defence Force Academy
Library

Newcastle
Library

New England
Library

Sydney
Engineering Library
Head, School of Civil Engineering

NSW
Physical Sciences Library
Professor R. A. A. Bryant, Mechanical Engineering

Queensland
Library

Tasmania
Engineering Library

Western Australia
Library
Associate Professor J. A. Cole, Mechanical Engineering

RMIT
Library

CANADA

CAARC Coordinator Structures
NRC
Aeronautical & Mechanical Engineering Library
Division of Mechanical Engineering, Director
Gas Dynamics Laboratory, Mr R. A. Tyler

Universities and Colleges
Toronto
Institute for Aerospace Studies

CZECHOSLOVAKIA
Aeronautical Research and Test Institute (Prague), Head

FRANCE
ONERA, Library

GERMANY
Fachinformationszentrum: Energie, Physic, Mathematik GMBH

INDIA
CAARC Coordinator Structures
Defence Ministry, Aero Development Establishment, Library
Gas Turbine Research Establishment, Director
Hindustan Aeronautics Ltd, Library
National Aeronautical Laboratory, Information Centre

INTERNATIONAL COMMITTEE ON AERONAUTICAL FATIGUE
per Australian ICAF Representative (25 copies)

ISRAEL
Technion-Israel Institute of Technology
Professot J. Singer
Dr I. T. Bar-Itzhack

ITALY
Professor Ing. Guiseppe Gabrielli

JAPAN
National Aerospace Laboratory
National Research Institute for Metals, Fatigue Testing Div.
Institute of Space and Astronautical Science, Library

Universities
Kagawa University
Professor H. Ishikawa

NETHERLANDS
National Aerospace Laboratory [NLR], Library

NEW ZEALAND
Defence Scientific Establishment, Library
RNZAF, Vice Consul (Defence Liaison)
Transport Ministry, Airworthiness Branch, Library

Universities
Canterbury
Library
Professor D. Stevenson, Mechanical Engineering

SWEDEN
Aeronautical Research Institute, Library
Swedish National Defence Research Institute (FOA)

SWITZERLAND

Armament Technology and Procurement Group
F+W (Swiss Federal Aircraft Factory)

UNITED KINGDOM

CAARC, Secretary
Royal Aircraft Establishment
  Bedford, Library
  Pyestock, Director
  Farnborough, Dr G. Wood, Materials Department
Commonwealth Air Transport Council Secretariat
Admiralty Research Establishment
  Holton Heath, Dr N. J. Wadsworth
  St Leonard's Hill, Superintendent
National Industrial Fuel Efficiency Service, Chief Engineer
National Physical Laboratory, Library
National Engineering Laboratory, Library
British Library, Document Supply Centre
CAARC Co-ordinator, Structures
Aircraft Research Association, Library
British Ship Research Assoication
NMI Limited (National Maritime Institute), Library
Electrical Power Engineering Company Ltd
Fulmer Research Institute Ltd, Research Director
Motor Industry Research Association, Director
Ricardo & Company Engineers (1927) Ltd, Manager
Rolls-Royce Ltd, Aero Division Bristol, Library
Welding Institute, Library
British Aerospace
  Kingston-upon-Thames, Library
  Hatfield-Chester Division, Library
British Hovercraft Corporation Ltd, Library
Short Brothers Ltd, Technical Library

Universities and Colleges

Bristol
  Engineering Library

Cambridge
  Library, Engineering Department
  Whittle Library

Manchester
  Professor, Applied Mathematics

Nottingham
  Science Library

Southampton
  Library

Strathclyde
  Library

Cranfield Inst. of Technology
Library

Imperial College
Aeronautics Library

UNITED STATES OF AMERICA

NASA Scientific and Technical Information Facility
Metals Information
The Chemical Abstracts Service
Allis Chalmers Corporation, Library
Boeing Company
Mr W. E. Binz
Mr J. C. McMillan
Kentex Research Library
United Technologies Corporation, Library
Lockheed-California Company
Lockheed Missiles and Space Company
Lockheed Georgia
McDonnell Aircraft Company, Library
Metals Abstracts, Editor
Nondestructive Testing Information Analysis Center

Universities and Colleges

Chicago
John Crerar Library

Florida
Aero Engineering Department
Professor D. C. Drucker

Iowa State
Dr G. K. Serovy, Mechanical Engineering

Iowa
Professor R. I. Stephens

Princeton
Professor G. L. Mellor, Mechanics

Massachusetts Inst. of Tech.
MIT Libraries

Spares (10 copies)

TOTAL (220 copies)

Department of Defence

DOCUMENT CONTROL DATA

1. a. AR No.	1. b. Establishment No.	2. Document Date	3. Task No.
AR-004-481	ARL-STRUC-R-420	July 1986	DST 82/008

4. Title	5. Security	6. No. Pages
EXPERIMENTAL AND THEORETICAL DETERMINATION OF J_{IC} FOR 2024-T351 ALUMINIUM ALLOY	a. document: Unclassified b. title: U. c. abstract: U.	22 7. No. Refs: 25

8. Author(s)	9. Downgrading Instructions
P. W. Beaver M. Heller T. V. Rose	—

10. Corporate Author and Address	11. Authority (*as appropriate*)
Aeronautical Research Laboratories P.O. Box 4331, Melbourne, Vic., 3001	a. Sponsor c. Downgrading b. Security d. Approval

12. Secondary Distribution (*of this document*)

Approved for public release

Overseas enquirers outside stated limitations should be referred through ASDIS, Defence Information Services Branch, Department of Defence, Campbell Park, CANBERRA, ACT, 2601.

13. a. This document may be ANNOUNCED in catalogues and awareness services available to . . .

No limitations

13. b. Citation for other purposes (*i.e. casual announcement*) may be (*select*) unrestricted (*or*) as for 13 a.

14. Descriptors	15. COSATI Group
Fracture tests	11060
Fracture (mechanics)	11130
Fracture properties	
Aluminium alloys	
J_{IC} test	

16. Abstract

The J-integral is an elastic-plastic fracture mechanics parameter which can be regarded as a measure of the intensity of the crack tip stress and strain fields, irrespective of the plastic zone size. The value of J at the onset of stable crack extension, J_{IC}, has been suggested as a fracture criterion for both large- and small-scale yielding conditions. In this work the value of J_{IC} for an extruded, medium-strength aluminium alloy, 2024-T351 bar, was determined using: (i) *the Hutchinson-Rice-Rosengren crack tip model and experimentally-determined crack tip strain profiles;* (ii) *a finite element-hybrid contour method,* (iii) *a modified linear elastic fracture mechanics approach, and* (iv) *the ASTM standard multiple- and single-specimen techniques. Agreement between the values obtained from the crack tip strain profile method, the two numerical methods and the multiple-specimen methods is good.*

This page is to be used to record information which is required by the Establishment for its own use but which will not be added to the DISTIS data base unless specifically requested.

16. Abstract (*Contd*)

The J_{1C} value determined by the single-specimen method is not valid as the amount of crack extension at each load level could not be determined to the accuracy required by the ASTM standard, using the recommended unloading compliance method.

17. Imprint

Aeronautical Research Laboratories, Melbourne

18. Document Series and Number	19. Cost Code	20. Type of Report and Period Covered
Structures Report 420	256900	

21. Computer Programs Used

22. Establishment File Ref(s)

END

DATE
FILMED

12 87